Polyhedron 28 (2009) 3628–3634

Contents lists available at ScienceDirect

Polyhedron

journal homepage: www.elsevier.com/locate/poly

Coordination polymer $[Li_2Co_2(Piv)_6(\mu\text{-}L)_2]_n$ (L = 2-amino-5-methylpyridine) as a new molecular precursor for $LiCoO_2$ cathode material

Mikhail Bykov [b], Anna Emelina [b], Mikhail Kiskin [a,*], Aleksei Sidorov [a], Grigory Aleksandrov [a], Artem Bogomyakov [c], Zhanna Dobrokhotova [a], Vladimir Novotortsev [a], Igor Eremenko [a]

[a] N.S. Kurnakov Institute of General and Inorganic Chemistry, Russian Academy of Sciences, Leninsky Prosp. 31, 119991 Moscow, GSP-1, Russian Federation
[b] Department of Chemistry, M.V. Lomonosov Moscow State University, 1 Leninskie Gory, 119992 Moscow, Russian Federation
[c] International Tomography Centre, Siberian Branch of the Russian Academy of Sciences, Institutskaya Str. 3a, 630090 Novosibirsk, Russian Federation

ARTICLE INFO

Article history:
Received 30 April 2009
Accepted 22 July 2009
Available online 15 August 2009

Keywords:
Cobalt
Lithium
Heterometallic complex
Coordination polymer
Carboxylate ligands
X-ray analysis
Magnetic properties
Thermal decomposition
Heat capacity
Phase transition

ABSTRACT

The solid-state thermolysis (420–450 °C) of the new heterometallic coordination polymer $[Li_2Co_2(Piv)_6(\mu\text{-}L)_2]_n$ (**1**, Piv is the anion of pivalic acid, L is 2-amino-5-methylpyridine) followed by annealing of the decomposition products at 500 °C was shown to afford $LiCoO_2$ in quantitative yield. Compound **1** was characterized by X-ray diffraction and magnetic measurements.

© 2009 Elsevier Ltd. All rights reserved.

1. Introduction

Mixed-oxide ceramics belong to an important class of solid-state materials used in modern electronics. Materials for positive electrodes in lithium-ion batteries occupy an important place among oxide ceramics. Lithium cobaltate used in batteries is prepared primarily by the direct solid-state synthesis from lithium oxide or hydroxide and cobalt carbonate or oxide at rather high temperatures [1–4]. The main drawbacks of this method are that this process is time and energy consuming and, what is most important, that the lithium content decreases because prolonged annealing leads to lithium evaporation. The sol–gel synthesis of this material with the use of metal salts (nitrates or acetates) in the presence of polybasic carboxylic acids [5–8] affords more homogeneous samples, reduces the time of thermal processing, and allows a decrease in the temperature for the synthesis of complex oxides with desired structures. Among other methods for the synthesis of lithiated cobalt oxide, the mechanochemical synthesis is worthy of note [9]. However, the mechanochemical synthesis of crystalline lithium cobaltate by the mechanical treatment of mixtures of LiOH with $Co(OH)_2$ and CoOOH followed by heating at 400–800 °C is complicated by the instability of the resulting $LiCO_2$ to the mechanochemical action due to redox processes with the involvement of the gas phase [10]. The compositional homogeneity and particle size uniformity are most important for the preparation of high-quality cathode materials, because these parameters have a great influence on the electrochemical characteristics of positive electrodes [5–7]. Actually, the two last-mentioned methods provide sufficient homogeneity upon mixing of the starting compounds, as well as compositional homogeneity and particle size uniformity. It was shown that highly dispersed $LiCoO_2$ powders exhibit good cyclic performance [11].

An alternative approach to the solution of the problem of preparing compositionally homogeneous lithium cobaltate (in particular as thin films or highly dispersed powders) can be based on the use of heterometallic coordination compounds containing cobalt and lithium atoms in a ratio of 1:1 as molecular precursors capable of generating lithium cobaltate through mild thermolysis (400–500 °C). This method can be efficiently used to prepare various materials. However, this strategy has not yet found extensive application. It should be noted that the possibility of preparing thin mixed-metal Cu–Co and Ni–Cu oxide films starting from cubane-like molecular heterometallic precursors has been examined in

* Corresponding author. Tel.: +7 495 955 4835; fax: +7 495 952 1279.
E-mail address: mkiskin@igic.ras.ru (M. Kiskin).

0277-5387/$ - see front matter © 2009 Elsevier Ltd. All rights reserved.
doi:10.1016/j.poly.2009.07.065

recent years [12]. Analogous approaches were employed to decompose complex heterometallic compounds with the composition $[Li(H_2O)M(N_2H_3CO_2)_3]\cdot 0.5H_2O$ (M = Co or Ni), which were considered as the only precursors for the preparation of layered $LiMO_2$ materials [13]. In this case, a very low yield of the starting molecular precursors presents a serious problem. Apparently, this precludes the extensive use of these precursors in thermal synthesis.

The aim of the present study was to search for new molecular systems capable of generating lithium cobaltate through mild thermolysis. The requirement for the organic components involved in the heterometallic complexes is that they can be easily eliminated with the retention of the ratio of metals in the final product.

2. Experimental

2.1. Synthesis

The new coordination polymer **1** was synthesised with the use of freshly distilled THF and MeCN. The starting cobalt pivalate $[Co(Piv)_2]_n$ was prepared according to a known procedure [14]. In the synthesis of complex **1**, commercial 2-amino-5-methylpyridine (Fluka) was used.

2.1.1. $[Li_2Co_2(Piv)_6(2\text{-amino-5-methylpyridine})_2]_n$ (**1**)

Tetrahydrofuran (40 ml) was added to a mixture of $[Co(Piv)_2]_n$ (0.5 g, 1.9 mmol), LiPiv (0.207 g, 1.9 mmol) and 2-amino-5-methylpyridine (0.205 g, 0.9 mmol). The reaction mixture was stirred at 60 °C for 20 min. The resulting brown solution was concentrated to 10 ml, MeCN (40 ml) was added, and the mixture was concentrated to 10 ml at 80 °C. The solution was kept at +5 °C for 24 h. Brown crystals suitable for X-ray diffraction were separated from the solution by decantation, washed with cold MeCN, and dried in air. The yield of crystals of **1** is 81% based on $[Co(Piv)_2]_n$. Found (%): C, 52.95; H, 7.35; N, 5.66. $C_{21}H_{35}CoLiN_2O_6$: C, 52.84; H, 7.39; N, 5.87. IR, ν/cm^{-1}: 3384 m, 3130 m, 2960 s, 2928 m, 2868 m, 1612 v.s, 1572 v.s, 1564 v.s, 1520 m, 1504 s, 1484 v.s, 1424 v.s, 1400 v.s, 1376 m, 1364 v.s, 1300 w, 1260 w, 1228 c, 1144 w, 1120 w, 1044 w, 1032 m, 972 m, 952 m, 936 m, 904 s, 848 m, 824 m, 800 s, 792 s, 764 s, 744 w, 664 m, 608 v.s, 568 s, 528 m, 452 v.s, 436 v.s, 416 v.s, 400 v.s.

2.2. Methods

The elemental analysis of complex **1** was carried out on a Carlo Erba analyzer in the Center of Collaborative Research of the N.S. Kurnakov Institute of General and Inorganic Chemistry of the Russian Academy of Sciences. The spectra were measured on a Specord M-80 IR spectrometer in KBr pellets. The magnetochemical measurements were performed on a MPMS-5S SQUID magnetometer (Quantum Design) in the 2–300 K temperature range at a magnetic field strength $H = 5$ kOe. The molar magnetic susceptibility χ was calculated taking into account the atomic diamagnetism according to the Pascal additive scheme. In the paramagnetic region, the effective magnetic moment was calculated by the equation $\mu_{eff} = [(3k/N_A\beta 2)\chi T]^{1/2} \approx (8\chi T)^{1/2}$, where k is the Boltzmann constant, N_A is Avogadro's number and β is the Bohr magneton.

2.3. X-ray data collection

The X-ray diffraction study of complex **1** was carried out on an Enraf Nonius CAD-4 diffractometer (λMo, graphite monochromator, ω-scanning technique, the scan step was 0.3°, the exposure time per frame was 10 s) according to a standard technique [15]. The structure of complex **1** was solved by direct methods and refined by the full-matrix least-squares method with anisotropic displacement parameters for all non-hydrogen atoms. The hydrogen atoms of the carbon-containing ligands were positioned geometrically and refined using a riding model. All calculations were carried out with the use of the SHELX97 program package [16]. The *tert*-butyl substituents at the carboxylate groups are partially disordered. The positions of all methyl carbon atoms in the disordered CMe_3 fragments were located in difference Fourier maps and refined with occupancies of 0.506(12) and 0.494(12) for the *tert*-butyl group at the atom C(1), 0.674(10) and 0.326(10) at the atom C(6), and 0.531(17) and 0.469(17) at the atom C(11). The crystallographic parameters for complex **1** at $T = 293$ K are as follows: $C_{21}H_{35}CoLiN_2O_6$, $fw = 477.38$, blue, prismatic, crystal size $0.45 \times 0.23 \times 0.25$ mm, monoclinic system, space group $P2_1/c$, $a = 12.4255(10)$ Å, $b = 22.1287(10)$ Å, $c = 9.4545(10)$ Å, $\beta = 103.253(10)°$, $V = 2530.4(4)$ Å^3, $\lambda = 0.71073$, $Z = 4$, $\rho_{calc} = 1.253$ g cm^{-3}, $\mu = 7.13$ cm^{-1}, 5775 measured reflections, 3113 reflections with $I > 4.0\sigma(I)$, $R_{int} = 0.0843$, $\theta_{max} = 26.97$, $GOF = 1.047$, R_1 ($I > 2\sigma(I)$) = 0.0502, wR_2 ($I > 2\sigma(I)$) = 0.1365, R_1 (all data) = 0.1173, wR_2 (all data) = 0.1663, $T_{min/max} = 0.9006/0.7397$ [17], full-matrix least-squares on F^2.

The X-ray powder diffraction analysis of the solid decomposition products in air was carried out on a G670 (HUBER) Guinier camera using CuKα1 radiation. The X-ray powder diffraction analysis of the solid decomposition products in an inert atmosphere was performed on a FR-552 monochromator chamber (CuKα1 radiation) using germanium as the internal standard (X-ray diffraction patterns were processed on an IZA-2 comparator with an accuracy of ±0.01 mm).

2.4. Thermal decomposition

The thermal decomposition of compound **1** was studied by differential scanning calorimetry (DSC) and thermogravimetry (TGA). The thermogravimetric measurements were performed in an artificial air flow (20 ml/min) and in an argon flow (20 ml/min) on a *NETZSCH TG 209 F1* instrument in alundum crucibles at a heating rate of 10 °C/min. The composition of the gas phase below 250 °C was studied on a QMS 403C Aëolos mass-spectrometric unit under TGA conditions. The ionizing electron energy was 70 eV; the largest determined mass number (the mass-to-charge ratio) was 300 amu. The weight of the samples for thermogravimetric experiments was 0.5–3 mg. The differential scanning calorimetry study, in a dry artificial air flow (O_2, 20.8%; CH_4, <0.0001%) and in an argon flow (Ar, >99.998%; O_2, 0.0002%; N_2, <0.001%; aqueous vapor, <0.0003%; CH_4, <0.0001%), was carried out on a *NETZSCH DSC 204 F1* calorimeter in aluminum cells at a heating rate of 10 °C/min. The weight of the samples was 4–10 mg. Each experiment was repeated at least three times. The temperature scales and the calorimeter were calibrated based on the phase transition temperatures of standard compounds (C_6H_{12}, Hg, KNO_3, In, Sn, Bi and CsCl; 99.99% purity; ISO/CD 11357-1). For the TGA and DSC experiments, the samples were weighed on a *SARTORIUS RESEARCH R 160P* analytical balance with an accuracy of 1×10^{-2} mg.

2.5. Heat capacity

The heat capacities were measured by DSC on a *NETZSCH 204 F1* instrument in a dry argon flow (10 ml/min) in the 123–373 K temperature range at a heating rate of 10 °C/min in aluminum specimen containers ($V = 56$ mm^3, $d = 6$ mm) equipped with lids with a hole (the ratio of the surface area of the bottom of the container to the surface area of the hole was about 36).

The average weight of the samples for heat capacity measurements was about 10 mg. The heat capacity was calculated in accordance with the *ASTM E 1269* standard by the equation:

$$C_{p,S} = \frac{m_{St}}{m_S}\frac{DSC_S - DSC_{BL}}{DSC_{St} - DSC_{BL}}C_{p,St} \quad (1)$$

where the indices S, St and BL refer to the cell containing the sample, the cell containing the standard compound, and the empty cell, respectively. Sapphire (m = 12.69 mg) was used as the standard. Four series of measurements were carried out. The results were processed statistically. The controlled cooling of the measuring cells was performed manually using a liquid-nitrogen cooling system.

The differential scanning calorimeter was calibrated against the heat flux with the use of sapphire as the standard (ISO/CD 11357-1) according to the equation:

$$E(T) = \frac{DSC_{St}(T) - DSC_{BL}(T)}{m_{St}C_{p,St}(T)\beta} \quad (2)$$

where the indices St and BL refer to the cell containing the standard and the empty cell, respectively, $E(T)$ is the temperature-dependent calibration coefficient, DSC is the experimental DSC signal, m is the mass, C_p is the isobaric heat capacity, and β is the heating rate of the furnace. The calibration against the heat flux was carried out before each measurement throughout the temperature range of interest. The experimental data were processed using the *NETZSCH Proteus Thermal Analysis* program package.

3. Results and discussion

3.1. Synthesis, structure and magnetic properties of the coordination polymer $[Li_2Co_2(Piv)_6(\mu\text{-}L)_2]_n$

We chose the product prepared by the reaction of polymeric cobalt(II) pivalate $[Co(Piv)_2]_n$, lithium pivalate LiPiv and 2-amino-5-methylpyridine (L) in the Co:Li:L ratio of 2:2:1 in THF as the possible molecular precursor for the synthesis of $LiCoO_2$. This reaction afforded a coordination polymer with the composition $[Li_2Co_2(Piv)_6(\mu\text{-}L)_2]_n$ (**1**) in high yield (81%).

According to X-ray diffraction data, compound **1** is a 1D polymer containing the heteronuclear fragment $\{Li_2Co_2(Piv)_6(\mu\text{-}L)_2\}$ as the elementary unit (Fig. 1). This fragment consists of two symmetrically arranged dinuclear units $\{LiCo(Piv)_3\}$, in which the cobalt and lithium atoms are linked by three non-equivalent bridging pivalate anions. The centrosymmetric repeating unit $\{Li_2Co_2(Piv)_6(\mu\text{-}L)_2\}$ contains the square O_2Li_2 fragment (Table 1). The polymer chain is formed by linking adjacent cobalt atoms from different repeating heteronuclear fragments $\{Li_2Co_2(Piv)_6(\mu\text{-}L)_2\}$ by two bridging 2-amino-5-methylpyridine molecules (Fig. 1, Table 1). In the elementary unit, each cobalt atom is coordinated by the pyridine nitrogen atom of one bridging N-donor ligand and the amino nitrogen atom of the bridging ligand from the adjacent fragment. The proton of the coordinated amino group is involved in hydrogen bonding with the oxygen atom of the bridging carboxylate group (Fig. 1, Table 1).

Table 1
Selected bond lengths [Å] and bond angles [°] for compound **1**.

Parameter	Value
Li(1A)–Li(1)–Co(1)	125.7(3)
Li(1)–Co(1)–N(1)	156.76(15)
Li(1)–Co(1)–N(2)	113.79(13)
Li(1)–O(6)–Li(1A)	88.7(3)
O–C–O (range)	119.3(3)–123.7(3)
Co(1)···Li(1)	3.074(5)
Li(1)···Li(1A)	2.709(11)
Co(1)–N(1)	2.131(3)
Co(1)–N(2A)	2.372(3)
Co(1)–O(1)	2.141(3)
Co(1)–O(2)	2.225(3)
Co(1)–O(3)	2.004(2)
Co(1)–O(5)	2.026(2)
Li(1)–O(2)	1.947(6)
Li(1)–O(4)	1.876(6)
Li(1)–O(6)	1.901(6)
Li(1)–O(6A)	1.973(6)
C–O (range)	1.234(4)–1.265(4)
N(2)···O(3)*	2.828(4)

* N(2)–H(2B)–O(3) 155.3°, H(2B)···O(3) 1.98 Å.

It should be noted that the distance between the cobalt atom and the nitrogen atom of the amino group (Co(1)–N(2)) is substantially elongated (2.372(3) Å), which is indicative of weak interactions between these atoms. This situation is typical of amino derivatives of pyridine serving as a bridging ligand in polynuclear cobalt-containing pivalates, and has been observed earlier [18,19].

The magnetic behavior of compound **1** is unusual. At room temperature, the effective magnetic moment of compound **1** is 4.77 μ_B (per cobalt atom) (Fig. 2), which is close to the known experimental values for high-spin Co^{II} atoms (S = 3/2) taking into account spin-orbital interactions (4.4–5.2 μ_B) [20]. The magnetic moment

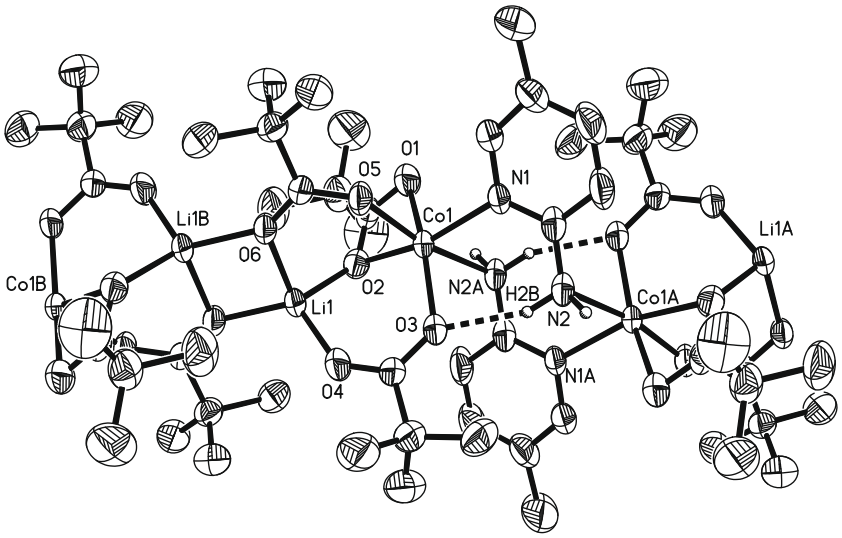

Fig. 1. Fragment of the polymer chain of compound **1** (only one component of each of the distorted *tert*-butyl groups is drawn, hydrogen atoms of the carboxylate and 2-amino-5-methylpyridine ligands (except for amino groups) are omitted for clarity, 50% thermal probability ellipsoids).

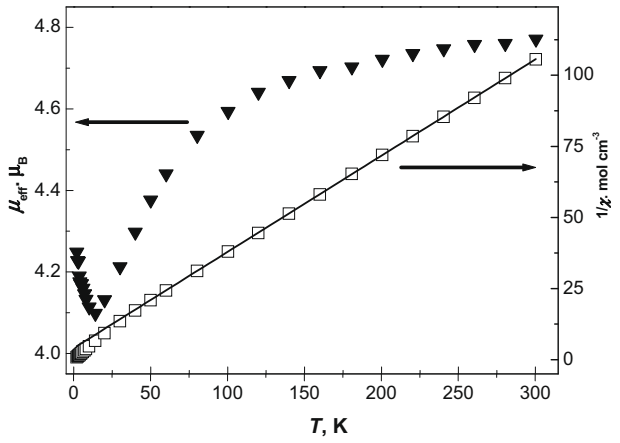

Fig. 2. Magnetic properties of complex **1**: the temperature dependence of the magnetic moment (▼), the curve $1/\chi$ (□); the calculated data are represented by the line.

μ_{eff} decreases with decreasing temperature (to 4.10 μ_B at 14 K). This fact can be attributed to both antiferromagnetic spin-spin exchange interactions between the cobalt atoms and the spin-orbital effect. However, μ_{eff} increases at temperatures below 14 K and reaches 4.25 μ_B at 2 K. Apparently, this effect is indicative of a ferromagnetic contribution to the exchange interactions between the Co^{II} atoms in the polymer chain.

In the 50–300 K temperature range, the temperature dependence of the inverse susceptibility follows the Curie–Weiss law with the parameters $C = 2.96$ mol cm^{-3} and $\theta = -11.96$ K (Fig. 2). The value $C = 2.96$ is larger than the theoretical pure spin value ($C = 1.875$ for $S = 3/2$ and $g = 2$), which is consistent with the orbital contribution to the magnetic susceptibility, typical of Co^{II} ions and g factors larger than 2.

3.2. Thermal decomposition

According to the TGA data, the decomposition of complex **1** in an artificial air flow and in a dry argon flow does not afford stable intermediates (Fig. 3).

The decomposition onset temperature for complex **1** is virtually the same (180 ± 3 °C) both in air and under an inert atmosphere (argon). The mass spectra of the gas phase in the 150–250 °C temperature range correspond to the spectrum of 2-amino-5-methylpyridine [21]. The initial step of decomposition of complex **1** (180–280 °C) is endothermic (the second endothermic peak in the DSC curves; see Fig. 3); the absorbed energy in air is 73.5 ± 5.3 kJ/mol per elementary unit of $Li_2Co_2(Piv)_6(L)_2$. The end of the second endothermic peak (260 ± 3 °C) corresponds to a 22.4 ± 1.5% weight loss. The number of 5-methyl-2-pyridineamine molecules calculated from the empirical formula is 22.67% per $Li_2Co_2(Piv)_6(L)_2$ formula unit. Presumably, heating in air in the above-mentioned temperature range leads to elimination of the N-donor ligand. Under an inert atmosphere, the endothermic effect in this temperature range has a complex character, and it is impossible to separate the thermal effect associated with elimination of the N-donor ligand. The inflection point in the weight loss curve at 280 ± 3 °C corresponds to a 21.7 ± 1.5% weight loss. At higher temperatures, further destructive decomposition of complex **1** is observed. It should be noted that the processes under an inert atmosphere differ from those in air. In an air flow, a highly exothermic oxidative destruction occurs in the 260–410 °C temperature range. The temperature of the end of the exothermic peak in air is virtually equal to the temperature of the end of the weight loss (Fig. 3b).

Under an inert atmosphere, the further weight loss occurs in the 280–470 °C temperature range. This process is accompanied by complex energy changes. According to the X-ray powder diffraction data, a heterogeneous mixture of cobalt oxide CoO and lithium oxide Li_2O is formed as the solid decomposition product of complex **1** under an inert atmosphere at temperatures below 500 °C (Table 2). The weight of the solid residue was 19.5 ± 1.5% of the weight of the starting sample, which agrees within experimental error to the value of 18.91% calculated from the empirical formula on the assumption that the decomposition affords a mixture of the Li_2O and CoO phases.

Unlike the inert conditions, the decomposition of polymer **1** in air (below 500 °C) affords a solid heterogeneous mixture of mixed-valence cobalt oxide Co_3O_4, lithium oxide Li_2O and lithium cobaltate $LiCoO_2$ (X-ray powder diffraction data; Table 2). However, the further storage of the thermolysis product under temperature-controlled conditions at 500 °C for 30–90 min led to the complete disappearance of the simple oxides, which is confirmed by the disappearance of reflections of the simple oxides in the X-ray diffraction patterns (Table 3). The weight of the solid residue upon thermolysis in air is 22.3 ± 1.5% of the weight of the starting sample, which agrees within experimental error to the value of 20.69% calculated from the empirical formula on the assumption that the decomposition affords $LiCoO_2$.

3.3. Heat capacity measurements

Differential scanning calorimetry studies showed that the endothermic effect in the 77–130 °C (350–405 K) temperature range

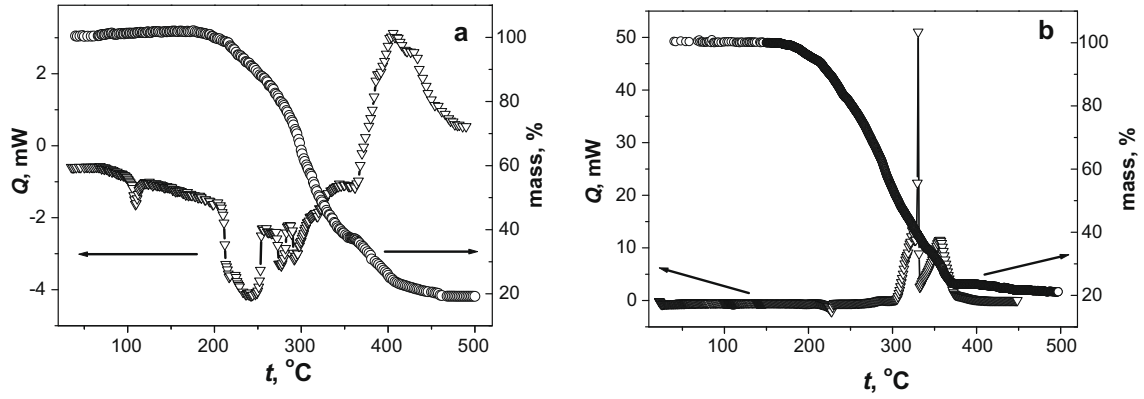

Fig. 3. Dependence of the weight loss (○) and the heat flux (▽) for the sample upon heating (*a*) under an inert atmosphere and (*b*) in an air flow.

Table 2
Phase analysis of the solid decomposition products of compound **1**.

Decomposition product under an inert atmosphere		Decomposition product in air without storage under temperature-controlled conditions		Li_2O [12–0254] *		CoO [48–1719]*		Co_3O_4 [43–1003]*		$LiCoO_2$ [50–653]*	
d (Å)	*I* (%)	*d* (Å)	*I* (%)	*d* (Å)	*I* (%)	*d* (Å)	*I* (%)	*d* (Å)	*I* (%)	*d* (Å)	*I* (%)
		4.695	100					4.667	16	4.6771	87
		2.850	20					2.858	33		
2.670	50			2.664	100						
2.455	50					2.4602	65				
		2.435	80					2.4374	100		
		2.410	40							2.4001	48
2.130	100					2.1307	100				
								2.0210	20		
		2.005	60							2.0019	100
1.650	20			1.6307	40						
		1.550	20					1.5558	32		
1.500	40					1.5066	54				
		1.395	20							1.4074	30

* *Powder Diffraction File*, Swarthmore: Joint Committee on Powder Diffraction Standards.

Table 3
Phase analysis of the solid decomposition product of compound **1** in air after storage under temperature-controlled conditions at 500 °C.

Decomposition product		$LiCoO_2$ [50-653]*	
d (Å)	*I* (%)	*d* (Å)	*I* (%)
4.695	100	4.6771	87
2.409	65	2.400	48
2.000	65	2.002	100
1.162	20	1.152	14

* *Powder Diffraction File*, Swarthmore: Joint Committee on Powder Diffraction Standards.

observed both under an inert atmosphere and in air is not associated with decomposition of the samples (Fig. 3) and is reproduced upon successive cooling and heating of the samples (Fig. 4).

To elucidate the nature of this thermal transformation, we measured the temperature dependence of the heat capacity. In addition, we intended to obtain thermodynamic characteristics for complex **1**, which are necessary for the construction of the thermodynamic model of the thermolysis. This model and the temperature program maintaining the constant level of gas evolution throughout the temperature range of thermolysis, which was calculated from the results of the thermal analysis, allow the optimization of the conditions for the preparation of lithium cobaltate films from the molecular precursor under consideration.

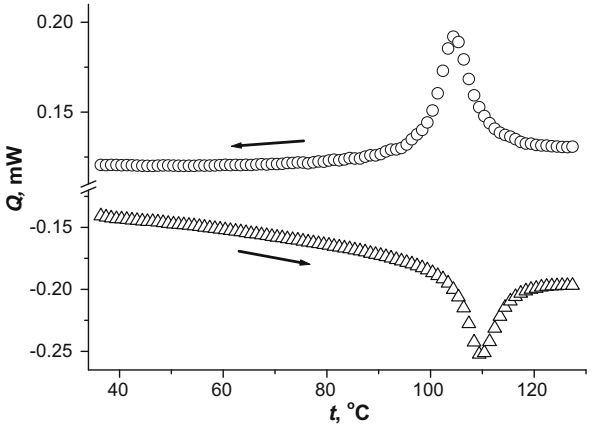

Fig. 4. Changes in the heat flux during heating (△) and cooling (○) of complex **1**.

The results of heat capacity measurements for complex **1** obtained by the statistical processing of experimental data are presented in Fig. 5. The experimental points deviate from the average smoothed curve by no more than 1.4%. The temperature dependence of C_p for complex **1** shows some anomalies. These anomalies are well reproduced, the characteristics of the anomalies being independent of the thermal history of the sample (anomaly 1: T_{onset} = 232.5 ± 0.5 K, Q = 79.1 ± 8.8 J/mol; anomaly 2: T_{onset} = 378.32 ± 0.26 K, Q = 6531 ± 715 J/mol).

According to the X-ray diffraction data, the crystal system and the space group of complex **1** remain unchanged in the 300–190 K temperature range (Table 4), but the unit cell parameters and the unit cell volume change non-monotonically. Hence, the low-temperature anomaly is presumably attributed to the phase transition associated with freezing of vibrations of the *tert*-butyl substituents at the carboxylate groups. Earlier, we have observed an analogous situation for the heteronuclear pivalate complex $Co_2Sm(Piv)_7(2,4\text{-}Lut)_2$ [22].

The endothermic effect in the 350–405 K temperature range is apparently attributed to the cleavage of a large number of hydrogen bonds formed between the protons of the coordinated amino group and the oxygen atoms of the bridging and chelate bridging carboxylate groups, accompanied by energy release. The thermal effect of this transformation is comparable with the hydrogen bond energy [23].

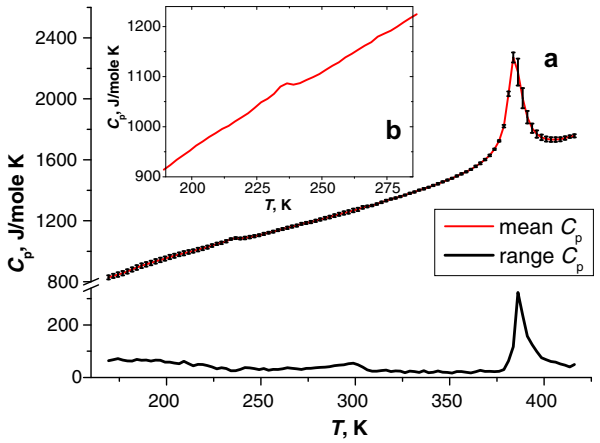

Fig. 5. Average smoothed curve $C_p(T)$, the confidence interval, and the difference between the maximum and minimum experimental values of C_p (*a*), the average smoothed curve $C_p(T)$ in the 190–280 K temperature range (*b*) (DSC, *HR* = 10 °C/min, Ar (10 ml/min), $m \sim 10$ mg).

Table 4
Unit cell parameters for compound **1** depending on the temperature.

T (K)	t (°C)	a (Å)	b (Å)	c (Å)	β (°)	V (Å^3)
403	130	12.596(14)	22.305(16)	9.537(6)	102.83(5)	2614(51)
300	27	12.568(18)	22.32(3)	9.534(13)	103.37(5)	2602(5)
280	7	12.476(12)	22.17(2)	9.461(9)	103.53(3)	2545(2)
260	−13	12.484(11)	22.20(2)	9.458(8)	103.67(5)	2547(5)
210	−63	12.430(7)	22.130(11)	9.366(5)	103.939(17)	2501(4)
190	−83	12.414(5)	22.122(8)	9.332(4)	103.931(17)	2487.4(1.5)

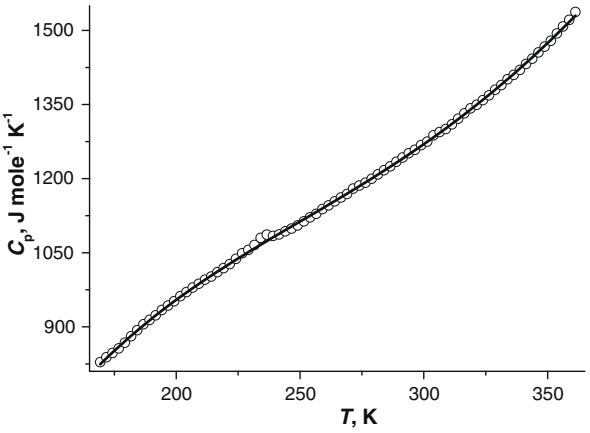

Fig. 6. Dependence of the heat capacity of complex **1**: experimental data (○); the calculated data are represented by the line (a_1 = 1396, θ_1 = 437, a_2 = 7779, θ_2 = 2617).

The absolute entropies of complex **1** were calculated from the limited region of the heat capacity curve (120–350 K) by extrapolating the results of DSC heat capacity measurements from the boiling point of liquid-nitrogen to the absolute zero temperature (0 K). This method gives the physically correct behavior of the temperature dependence of the heat capacity and the mathematically correct standard entropies [22]. To calculate the thermodynamic functions of the complexes, we separated the regular heat capacity contribution and approximated it to 0 by the function:

$$c_p(T) = \sum_i a_i C_{En}\left(\frac{\theta_i}{T}\right) \quad (3)$$

$$\text{where} \quad C_{En}(x) = 3Rx^2\frac{\exp(x)}{[\exp(x)-1]^2}, \quad x = \frac{\theta}{T}$$

The best results were obtained by approximating with function (3), consisting of two summands (Fig. 6).

The standard entropies S^o_{298} of the complexes were estimated by the equation:

$$S(T) = \sum_i a_i S_{En}\left(\frac{\theta_i}{T}\right) \quad (4)$$

$$\text{where} \quad S_{En}(x) = 3R\left[\frac{x}{(\exp(x)-1)} - \ln(1-\exp(-x))\right], \quad x = \frac{\theta}{T}.$$

We took into account the change in the entropy as a result of the transition associated with the anomaly in the curve for C_p according to the equation $\Delta S^{\circ}_{T_{onset}} = \frac{AREA}{T_{onset}}$, where AREA is the measured surface area of the peak in the experimental temperature dependence of the heat capacity. Table 5 gives the experimental (average and smoothed) heat capacities, the temperature contributions to the enthalpy calculated from the heat capacities, and the standard entropies (the latter parameters were determined with the use of the calculated value of S^o_{298}).

Table 5
Thermodynamic functions of compound **1**.

T (K)	C_p (±11.1) (J/mol K)	$H^o_T - H^o_{170}$ (kJ/mol)	S^o_T (J/mol K)
170	828.5	0	403
180	867.8	8.4	451
190	914.2	17.3	500
200	952.0	26.7	547
210	987.2	36.3	595
220	1018.7	46.3	642
250	1105.2	78.3	778
260	1138.5	89.5	822
270	1168.8	101.0	866
280	1199.8	112.8	909
290	1234.0	124.9	952
298	1267.7	137.4	994
310	1300.4	150.2	1036
320	1342.3	163.4	1078
330	1380.1	177.0	1120
340	1420.0	190.9	1162
350	1467.2	205.3	1204

Hence, the study of the heat capacity of coordination polymer **1** in the 123–373 K temperature range revealed two anomalies associated with phase transitions. The parameters of these transitions were determined. The thermodynamic functions ($C^o_p(T)$, $S^0(T)$ and $H^0(T)$–$H^0(170)$) in the 170−350 K temperature range were calculated based on the results of the calorimetric measurements.

4. Conclusions

The above-considered data show that the new heterometallic coordination polymer **1** can apparently be used as an efficient molecular precursor for the synthesis of lithium cobaltate. Under the conditions of the experiments (heating at a rate of 10 °C/min), $LiCoO_2$ can be prepared as the only solid thermolysis product, only after additional storage under temperature-controlled conditions at 500 °C. Preliminary investigations into the preparation of films from saturated solutions of complex **1** on different supports (an alundum support, a stabilized zirconium dioxide support and a sapphire support) showed that homogeneous uniform $LiCoO_2$ films can be formed with the use of a temperature program, which was calculated from the kinetic model of the thermolysis of complex **1**, designed based on the results of thermal analysis and which maintains a constant (3%/min) gas evolution rate during decomposition of coordination polymer **1**.

Supplementary data

CCDC 730046 contains the supplementary crystallographic data for compound **1**. These data can be obtained free of charge via http://www.ccdc.cam.ac.uk/conts/retrieving.html, or from the Cambridge Crystallographic Data Centre, 12 Union Road, Cam-

bridge CB2 1EZ, UK; fax: (+44) 1223-336-033; or e-mail: deposit@ccdc.cam.ac.uk.

Acknowledgments

This study was supported by the Russian Foundation for Basic Research (project nos. 07-03-00707, 08-03-00091, 09-03-90441, 09-03-12228, 09-03-12122, and 08-03-00343), the Council on Grants of the President of the Russian Federation (grants NSh-1324.2008.3, NSh-1518.2008.3, MK-156.2009.3), the Federal Agency for Science and Innovations, the Russian Science Support Foundation, the Russian Academy of Science, the Siberian Branch of the Russian Academy of Sciences and the Department of Chemistry and Materials Science.

References

[1] J.N. Reimers, J.R. Dahn, J. Electrochem. Soc. 139 (1992) 2091.
[2] T. Ohzuku, A. Ueda, J. Electrochem. Soc. 141 (1994) 2972.
[3] M. Wang, A. Navrotsky, J. Solid State Chem. 178 (2005) 1230.
[4] B. Garcia, J. Farcy, J.P. Pereira-Ramos, J. Perichon, N. Baffier, J. Power Sources 54 (1995) 373.
[5] Z.S. Peng, C.R. Wan, C.Y. Jaing, J. Power Sources 72 (1998) 215.
[6] S. Myung, N. Kumagai, S. Komaba, J. Appl. Electrochem. 30 (2000) 1081.
[7] C. Julien, S. Gastro-Garsia, J. Power Sources 97–98 (2001) 290.
[8] C.-C. Chang, P.N. Kumta, J. Power Sources 75 (1998) 44.
[9] W. Jang, Y. Lee, K. Baik, M. Lee, Mater. Res. Bull. 38 (2003) 1.
[10] N.V. Kosova, T.V. Larina, E.T. Devyatkina, J. Chem. Sustain. Develop. (2001) 235.
[11] K. Kanamura, A. Goto, R. Young Ho, T. Umegaki, K. Toyoshima, K. Okada, Y. Hakuta, T. Adschiri, K. Aria, Electrochem. Solid-State. Lett. 3 (2000) 256.
[12] M. Hamid, A.A. Tahir, M. Mazhar, M. Zeller, K.C. Molloy, A.D. Hunter, Inorg. Chem. 45 (2006) 10457.
[13] S.L. Tey, M.V. Reddy, G.V.S. Rao, B.V.R. Chowdari, J.J. Ding, J.J. Vittal, Chem. Mater. 18 (2006) 1587.
[14] M.A. Golubnichaya, A.A. Sidorov, I.G. Fomina, M.O. Ponina, S.M. Deomidov, S.E. Nefedov, I.L. Eremenko, I.I. Moiseev, Russ. Chem. Bull. (Engl. Transl.) 48 (1999) 1751.
[15] SMART (Control) and SAINT (Integration) Software, Version 5.0, Bruker AXS Inc., Madison, WI, 1997.
[16] G.M. Sheldrick, SHELX97, Program for the Solution of Crystal Structures, Göttingen University, Götinngen, Germany, 1997.
[17] G.M. Sheldrick, SADABS, Program for Scanning and Correction of Area Detector Data, Göttingen University, Göttinngen, Germany, 1997.
[18] E.V. Pakhmutova, A.E. Malkov, T.B. Mikhailova, A.A. Sidorov, I.G. Fomina, G.G. Aleksandrov, V.M. Novotortsev, V.N. Ikorskii, I.L. Eremenko, Russ. Chem. Bull. Int. Ed. 52 (2003) 2117.
[19] E.V. Pakhmutova, A.E. Malkov, T.B. Mikhailova, I.G. Fomina, A.A. Sidorov, G.G. Aleksandrov, I.F. Golovaneva, V.M. Novotortsev, V.N. Ikorskii, S.E. Nefedov, I.L. Eremenko, Russ. Chem. Bull. Int. Ed. 52 (2003) 139.
[20] Yu.V. Rakitin, V.T. Kalinnikov, Sovremennaya magnetokhimiya (Nauka. St-Petersburg, 1994), Modern magnetochemistry, Science, St. Petersburg, 1994 (in Russian).
[21] http://webbook.nist.gov.
[22] M.A. Bykov, A.L. Emelina, M.A. Kiskin, G.G. Aleksandrov, A.S. Bogomyakov, Zh.V. Dobrokhotova, V.M. Novotortsev, I.L. Eremenko, Russ. J. Inorg. Chem. Int. Ed. 54 (2009) 548.
[23] A. Albinati, V.I. Bakhmutov, N.V. Belkova, C. Bianchini, I. de los Rios, L. Epstein, E.I. Gutsul, L. Marvelli, M. Peruzzini, R. Rossi, E. Shubina, E.V. Vorontsov, F. Zanobini, Eur. J. Inorg. Chem. (2002) 1530.